Shocks in Inertial Dewetting

A. Buguin,[1] L. Vovelle,[2] and F. Brochard-Wyart[1]
[1]*Institut Curie, P.C.C-UMR 168, 11, Rue Pierre et Marie Curie, 75231 Paris Cedex 05, France*
[2]*Rhône Poulenc, 85, Avenue des Frères Perret, BP 62, 69192 St. Fons, France*
(Received 22 December 1998)

We present the first observation of a shock in the fast dewetting of a water film (thickness e) from hydrophobic glass. The film dewets by the nucleation and growth of a dry patch (velocity V), surrounded by a rim which collects the liquid. The velocity of dewetting $V(e)$ follows the Culik law for the bursting of soap films, with a driving force including both capillarity and gravity. The profile of the rim is measured by the deflection of a laser beam. The shock is observed when the rim surfs on the immobile film at velocities $V^* > \sqrt{ge}$, the velocity of gravity waves (g = gravitational acceleration) in shallow water. Ripples emitted in front of the rim give us a signature of the shock.

PACS numbers: 68.15.+e, 47.35.+i, 68.45.Gd

When a hydrophobic surface is covered by a water film, dry regions appear and grow: This is called dewetting. It may occur either by spinodal decomposition [1,2] or by nucleation and growth [3]. Dewetting has important practical applications: it governs (a) spontaneous drying [4], (b) the hydroplaning of cars [5] (dewetting between asphalt and rubber), (c) the operation of four-color-offset printing [6] (dewetting between roller and paper), or (d) the protection of plants by fungicides in water (where dewetting must be blocked).

The slow dewetting of viscous liquids has been studied in detail. It involves a small rim ahead of the dry region, where the liquid is collected. The shape and the viscous losses of the rim are now well known [3,7]. In this Letter, we concentrate on the opposite limit: nearly inviscid liquids, and relatively large film thicknesses e, leading to large velocities [8,9] and to completely different water profiles. Our experimental system is a large sheet (20×20 cm) of float glass, covered by a molecular carpet of octadecyltrichlorosilane, following the method of Ref. [10]. The driving force is a negative spreading coefficient [11], expressing the fact that the solid surface prefers to be dry,

$$S = \gamma_{SO} - (\gamma + \gamma_{SL}) = -\frac{1}{2}\rho g e_c^2 = -82 \text{ mN/m}. \tag{1}$$

In Eq. (1) γ_{SO} (γ_{SL}) is the interfacial energy between solid and air (water), γ is the water surface tension, and $e_c = 3.9$ mm is the critical thickness above which gravity prevents dewetting (ρ = density; g = gravitational acceleration) [3]. For $e < e_c$, our films dewet by nucleation and growth of a dry patch. We induce the nucleation (at $t = 0$) by dipping a Teflon tip at the center of the film.

Dewetting is observed with a video camera (25 images/s): We measure the front velocity V^* of the advancing rim and the velocity V for the growth of the dry patch (V^* and V are time independent). Two dimensionless parameters are important:

(a) a Reynolds number:

$$\text{Re} = \frac{V_e e}{\nu} = \frac{g^{1/2} e^{3/2}}{\nu} \cong 10^2, \tag{2}$$

where V_e is a characteristic velocity, which for our purposes is comparable to the velocity of capillary waves in shallow water $V_e = \sqrt{ge}$ and $\nu = \frac{\eta}{\rho}$ is the kinematic viscosity.

(b) a Froude number:

$$\text{Fr} = \frac{V^*}{\sqrt{ge}}. \tag{3}$$

In all our measurements Fr is larger than unity. This implies that the front is a shallow water shock as proposed in Ref. [12], similar to the hydraulic jump observed at the bottom of a sink.

If we assume that the water rim has a constant thickness h between the dry patch radius R_d and the shock radius R_s (Fig. 1), we find two classical Rankine-Hugoniot conditions:

(i) mass conservation:

$$h(V^{*2} - V^2) = eV^{*2}. \tag{4}$$

(ii) momentum conservation:

$$eV^* V_1 = \frac{1}{2} g(h^2 - e^2), \tag{5}$$

where $V_1 = VR_d/R_s = V^2/V_s$ is the liquid velocity in the rim at radius R_s. Equations (4) and (5) lead to

$$\begin{cases} V^2 = \dfrac{1}{2} g \dfrac{h^2 - e^2}{e}, \\ V^{*2} = \dfrac{1}{2} g \dfrac{h(e + h)}{e}. \end{cases} \tag{6}$$

If we set $h = e_c$ in Eq. (6), the velocity of dewetting V is similar to the Taylor-Culik [13] law for the bursting of soap film, with a driving force,

$$-\tilde{S} = \gamma_{SL} + \gamma - \gamma_{SO} - \frac{1}{2}\rho g e^2 = \frac{1}{2}\rho g(e_c^2 - e^2), \tag{7}$$

instead of 2γ for a suspended film.

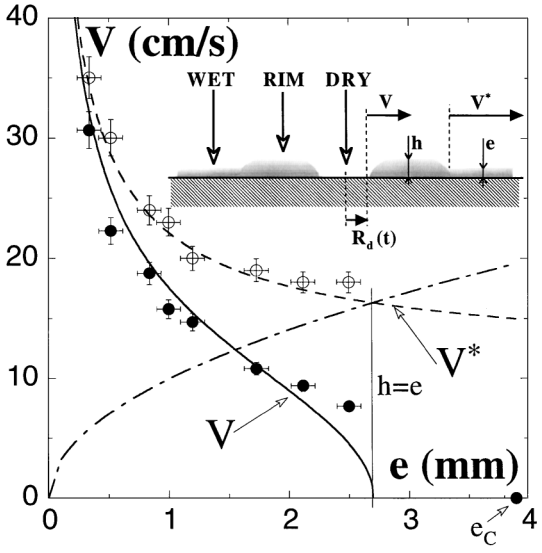

FIG. 1. Evolution of the velocity V (solid circle) for the growth of the dry patch and front velocity V^* (open circle) of the advancing film versus the film thickness e. Our results are fitted by Eq. (6) (solid line and dotted line). $\sqrt{ge}$ is drawn as a pointed line for comparison. The inset shows a chemical representation of the film during dewetting.

Experimental curves for V and V^* fit Eq. (6), with $h = 2.7$ mm (Fig. 1). This thickness h is different from $e_c = 3.9$ mm. The Culik law is observed, but the dynamic spreading parameter ($S_d = -35\ \mathrm{mN\,m^{-1}}$) is significantly different from the static value ($S = -82\ \mathrm{mN\,m^{-1}}$). This means that a part of the surface energy is lost in another process.

To characterize the shock, we need to measure the profile of the film around the expanding dry patch. We are faced with two difficulties: the high speed (up to 0.5 m/s) and the range of thickness, which excludes interferometry techniques. This led us to a different approach; at a given point of the interface, we measure the deflection of a laser beam by the rippled water surface. The setup is sketched in Fig. 2. We obtain the local slope angle $\theta(R, t)$. Because the front velocity V^* is time independent, we may reconstruct the profile $h(t)$ near the shock as follows:

$$h(R,t) = e + \int_0^t \tan[\theta(R,t)]V^*\,dt\,. \qquad (8)$$

We show in Fig. 3 typical profiles during the dewetting at various distances from the nucleation point and for different thicknesses e of the liquid film. To test the validity of the profiles, we check the volume conservation. The liquid volume which has dewetted ($V_{\mathrm{th}} = \pi R_d^2 e$) is compared to the volume measured on the profiles ($V_{\mathrm{mes}} = 2\pi \int_{R_d}^{\infty}(h - e)r\,dr$). Volume conservation is verified within 4%.

To follow the evolution of the shock with time, we first analyze the rim profile versus the distance R from the nucleation point. The profiles at five distances (from 2.2 to 8 cm) are shown in Fig. 3(a) for a film of

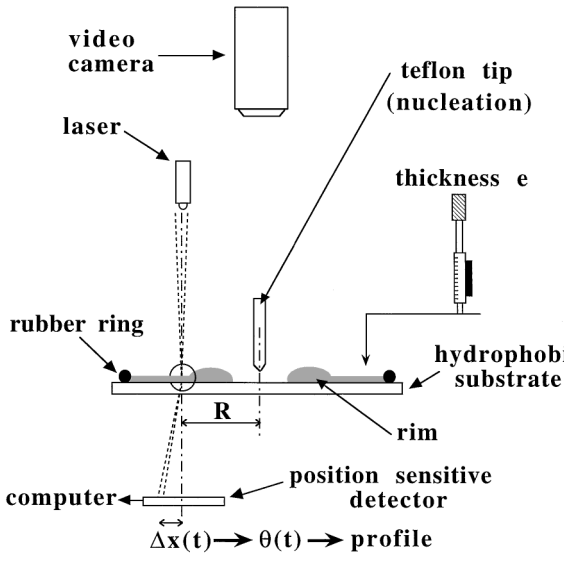

FIG. 2. Experimental setup to observe and characterize the profile of the bursting film on a silanized glass plate.

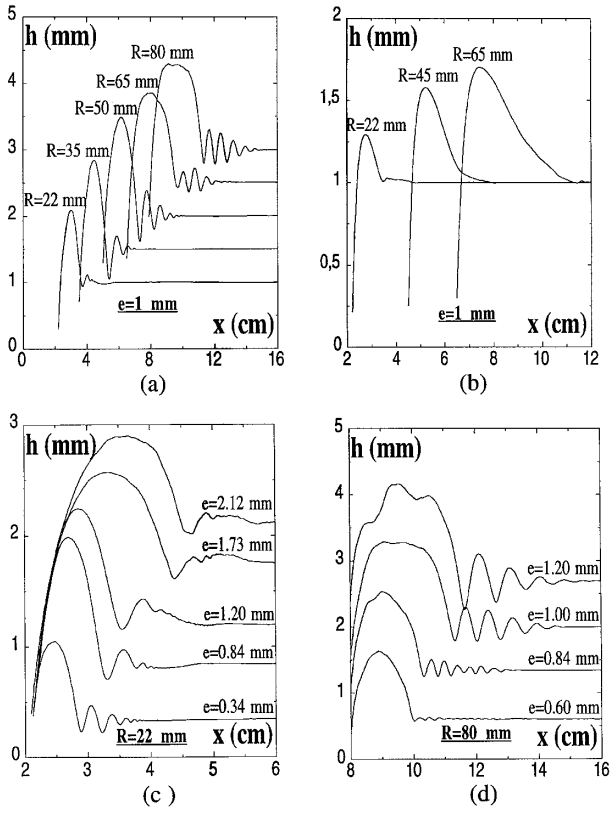

FIG. 3. Profiles $h(x)$ of rims and waves. (a) Versus time (or equivalent distance from the nucleation point): in this case the profiles are shifted by $\Delta h = 0.5$ mm for clarity. (b) At Froude number Fr < 1: notice the absence of ripples. (c) Versus thickness at a distance $R = 2.2$ cm from the nucleation point. (d) Versus thickness at a distance $R = 8$ cm from the nucleation point: in this case the profiles are shifted by $\Delta h = 0.5$ mm for clarity.

initial thickness $e = 1.0 \pm 0.1$ mm. The rim generates capillary waves in the native film. The extension of these ripples increases with time, but the wavelength remains constant ($\lambda = 2\pi/k = 7.6$ mm). The rim is almost circular at short distances and gets larger and becomes flat: its thickness (2.3 mm at a distance $R = 8$ cm) is close to the value $h = 2.7$ mm derived from the fit of V and V^* with Eq. (6).

We then investigate the influence of varying film thickness on the shock. The profile shape at a distance $R = 22$ mm from the nucleation point for five thicknesses is shown in Fig. 3(c). The capillary waves are clearly apparent only for small thicknesses e. The same measurements performed at $R = 80$ mm from the nucleation point are shown in Fig. 3(d). Now the waves ahead of the rim are well formed. One notices that the amplitude and the wavelength decrease as the thickness e decreases. For the thickest film ($e = 1.2$ mm), the rim is not flat. This is due to wave reflection at the outer circular ring. It is thus impossible to determine the profiles for larger thicknesses at $R = 80$ mm.

The waves generated by the rim are capillary gravity waves in shallow water. Their phase velocity c_φ should be equal to the velocity V^* [9]. We can measure directly from the profiles the wave vector $k = 2\pi/\lambda$ and compute c_φ using the dispersion equation of capillary waves in shallow water in the inertial regime,

$$c_\varphi^2 = \frac{g}{k}\tanh(ke)[1 + (k/\kappa)^2], \qquad (9)$$

where $\kappa^{-1} = 2.7$ mm.

From the plots of c_φ, V^* versus e, we have checked that the resulting values of c_φ are in good agreement with the measured values V^*. The condition $c_\varphi = V^*$ implies from Eq. (9) that the wavelength λ is constant in time during the dewetting process [as seen in Fig. 3(a)] and increases with thickness [as clearly seen in Fig. 3(d)].

The influence of the Froude number is obvious if we compare Figs. 3(a) and 3(b). Figure 3(b) shows the rim profile obtained with a more viscous liquid for which the dewetting velocity does not satisfy the shock conditions. The liquid used is a water/glycerol (50%/50%) solution which is about 6 times more viscous than water. For a film thickness $e = 1$ mm, the measured velocity for the external radius of the rim is $V^* = 6$ cm/s $< \sqrt{ge} = 10$ cm/s. The Froude number is now smaller than 1, whereas the Reynolds number is still large (of the order of 20). The waves have disappeared: They are clearly a signature of the shock. Notice also that the shape of the rim is very asymmetric and more smooth on the liquid side.

From all these measurements, we conclude that the front velocity V^* and the rim thickness h do obey the Hugoniot relation [Eq. (6)], but the magnitude of h does not follow the predictions of Ref. [12], which postulates that $h = e_c$ (= 3.9 mm). We have investigated a number of reasons for this discrepancy.

(i) *Viscous losses in the boundary layer and at the contract line.*—To compute the dewetting velocity by the Culik law, we neglected the viscous forces exerted by the substrate on the rim assuming a very large Reynolds number. Nevertheless, with a boundary layer model, it is possible to evaluate this force. The dissipation in this viscous boundary layer per unit length and per unit time is

$$T\dot{S} = f_V V \cong \eta \int_0^1 \left(\frac{V}{\delta(x)}\right)^2 \delta(x)\, dx\,, \qquad (10)$$

where $\delta(x) = \sqrt{\nu x/V}$ is the thickness of the boundary layer at distance x from the front and $1 = R_s - R_d$ is the width of the rim. Integration of Eq. (10) leads to $f_V \cong \rho V^2\sqrt{\nu 1/V}$. Taking a water rim 1 cm long and a dewetting velocity of 20 cm/s gives a viscous force of the order of 10 mN/m. This term becomes significant for extended rims. On the other hand, we have checked that the viscous losses in the liquid wedge at the contact line are entirely negligible.

(ii) *Wave resistance* [9].—The capillary waves generated ahead of the rim carry a part of the surface energy. This energy per unit time $\dot{E}$ is [14]

$$\dot{E} = E(c_g - c_\varphi)\,, \qquad (11)$$

where c_g is the group velocity, c_φ is the phase velocity of the capillary waves of amplitude a, and E is the wave energy per unit area, $E = \frac{1}{2}\rho c_\varphi^2[k/\mathrm{th}(ke)]a^2$. From Eq. (11), we can define the wave resistance $\mathcal{R}$ acting on the rim moving at velocity c_φ by the relation $\dot{E} = \mathcal{R}c_\varphi$, which leads to $\mathcal{R} = \frac{1}{2}\rho c_\varphi^2[k/\mathrm{th}(ke)]a^2(c_g/c_\varphi - 1) = \frac{1}{2}\gamma\kappa^2 a^2$. With $e = 1$ mm, $k \approx 1$ mm^{-1}, $a \approx 0.1$ mm, and $\gamma = 72$ mN/m, we obtain $\mathcal{R} = 0.5$ mN/m. This wave resistance is too weak to change the dewetting kinetics.

(iii) *Nature of the driving force F_d* [15].—We have evaluated F_d by taking into account the interfacial tensions acting on the rim and the hydrostatic pressure on the forward side, giving $F_d = \frac{1}{2}\rho g(e_c^2 - e^2)$. This may be naive, because the rim is a deformable object which extends with time; calculating the change of potential energy versus time, we have reached [15] another expression for the driving force, $F_d = \frac{1}{2}\rho g(e_c^2 - eh)$. Used in conjunction with the Hugoniot equation (6), this leads to lower thicknesses h defined by the condition $h^2 - e^2 = e_c^2 - eh$. For $e = 1$ mm the predicted h is then $h = 3.5$ mm as compared to $h_{\mathrm{exp}} = 2.7$ mm. Moreover the Culik law [$F_d = (dM/dt)V$] assumes that the rim moves at uniform velocity. In the limit $V^* > V$, one cannot neglect the spatial variation of velocity when evaluating the momentum of the whole rim. The net effect is also a reduction of h, which may be more significant [15].

Our central conclusion is that the dewetting of millimetric films is dominantly inertial and associated with a shock wave. It is of interest to compare the bursting of our supported films with the inertial bursting of (nonsupported)

soap films. At first sight, the supported films appear more complex; they must have a laminar boundary layer near the solid wall. However, the soap films are more delicate: They have surfactant monolayers on their surface, and these layers transport another form of shock waves, first analyzed by Frankel [16]. The dynamics depends on the pressure relations inside a monolayer.

Horizontal suspended films are unsensitive to gravity: The Froude number is always very large. The shock condition is always satisfied and ripples surrounded the film should be present. They have not been observed experimentally, but they show up in the numerical simulations of the bursting of *bare* (with no surfactants) suspended films [17]. Supported films have an adjustable Froude number Fr. We can vary the driving force $\tilde{S}$ and the Froude number by changing the thickness. When $\mathrm{Fr} > 1$, we have a shock preceded by ripples. When $\mathrm{Fr} < 1$, there is no shock. Supported films provide us with a tunable generator of shocks.

We are indebted to E. Raphaël, P. G. de Gennes, P. Nassoy, and T. Duke for fruitful discussions.

[1] G. Reiter, Science **282**, 888 (1998).
[2] R. Xie, A. Karim, J. F. Douglas, C. C. Han, and R. A. Weiss, Phys. Rev. Lett. **81**, 1251 (1998).
[3] C. Redon, F. Brochard-Wyart, and F. Rondelez, Phys. Rev. Lett. **66**, 175 (1991).
[4] *Soft Matter Physics*, edited by M. Daoud and C. Williams (Springer-Verlag, Berlin, 1998).
[5] P. Martin and F. Brochard-Wyart, Phys. Rev. Lett. **80**, 3296 (1998).
[6] P. G. de Gennes, C.R. Acad. Sci. Ser. Gen., Ser. 2 **318**, 1033 (1994).
[7] F. Brochard-Wyart and P. G. de Gennes, Adv. Colloid Interface Sci. **39**, 1 (1992).
[8] C. Andrieu, C. Sykes, and F. Brochard-Wyart, J. Adhes. **58**, 15 (1996).
[9] F. Brochard-Wyart, E. Raphael, and L. Vovelle, C.R. Acad. Sci. Ser. Gen., Ser. 2 **321**, 367 (1995).
[10] J. Sagiv, J. Am. Chem. Soc. **102**, 92 (1980).
[11] P. G. de Gennes, Rev. Mod. Phys. **3**, 57 (1985).
[12] F. Brochard-Wyart and P. G. de Gennes, C.R. Acad. Sci. Ser. Gen., Ser. 2 **257**, 324 (1997).
[13] F. E. Culik, J. Appl. Phys. **31**, 1128 (1960).
[14] J. Lighthill, *Waves in Fluids* (Cambridge University Press, Cambridge, England, 1978).
[15] F. Brochard and A. Buguin, C.R. Acad. Sci. Ser. Gen., Ser. 2 (to be published).
[16] S. Frankel and K. Mysels, J. Phys. Chem. **73**, 3028 (1969).
[17] M. P. Brenner and D. Gueyffier, Phys. Fluids A **11**, 373 (1999).